Acta Oceanol. Sin., 2023, Vol. 42, No. 9, P. 53–61
https://doi.org/10.1007/s13131-023-2155-0
http://www.aosocean.com
E-mail: ocean2@hyxb.org.cn

Multi-proxy reconstructions of hydrological changes from continental shelf sediments in the northern South China Sea during the interval 9 200–6 200 cal a BP

Chao Huang[1, 2, 3], Xiaoxu Qu[1, 2], Lihui Wang[1, 2], Yuhan Xie[1, 2], Yongyi Luo[1, 2], Fajin Chen[1, 2, 3]*, Yin Yang[1, 2]

[1] Laboratory for Coastal Ocean Variation and Disaster Prediction, College of Ocean and Meteorology, Guangdong Ocean University, Zhanjiang 524088, China

[2] Key Laboratory of Climate, Resources and Environment in Continental Shelf Sea and Deep Sea of Department of Education of Guangdong Province, Guangdong Ocean University, Zhanjiang 524088, China

[3] Key Laboratory of Space Ocean Remote Sensing and Application, Ministry of Natural Resources, Beijing 100081, China

Received 3 August 2022; accepted 28 October 2022

Abstract

Past hydroclimatic conditions in southern China are poorly constrained owing to the lack of high-resolution marine-sediment records. In this study, we present high-resolution geochemical and grain-size records of marine sediments from the coastal shelf of the northern South China Sea to investigate regional hydrological variations. Results suggest a warm and humid climate during the interval 9 200–7 600 cal a BP, followed by a cold and dry climate from 7 600 cal a BP to 6 500 cal a BP, and progressive humidification during the period 6 500–6 200 cal a BP. A prominent hydrological anomaly occurred during 7 600–6 500 cal a BP. This abrupt event corresponds closely to tropical Pacific and interhemispheric temperature gradients, suggesting that moisture variations in southern China may have been driven by interhemispheric and zonal Pacific temperature gradients via modulation of the intensity and location of the West Pacific subtropical high.

Key words: South China Sea, Holocene, East Asian summer monsoon, chemical weathering

Citation: Huang Chao, Qu Xiaoxu, Wang Lihui, Xie Yuhan, Luo Yongyi, Chen Fajin, Yang Yin. 2023. Multi-proxy reconstructions of hydrological changes from continental shelf sediments in the northern South China Sea during the interval 9 200–6 200 cal a BP. Acta Oceanologica Sinica, 42(9): 53–61, doi: 10.1007/s13131-023-2155-0

1 Introduction

The Asian summer monsoon (ASM) is an integral part of the global climate system and exerts a significant influence on the hydrology and ecology of the Asian region, as well as on the population living there (IPCC, 2021; Yang et al., 2008; Zhang et al., 2011). In the context of modern global climatic change, the monsoonal climate in China is showing increasing regional differences, including more frequent extreme precipitation events and droughts that affect regional economic activity and livelihoods. An understanding of the nature of monsoon rainfall and its forcing on timescales longer than those of the instrumental record is essential for understanding present climatic conditions and predicting future climate change.

The variation in monsoon rainfall on different timescales has been investigated previously (Ding et al., 2008; Huang et al., 2019; Lu et al., 2021; Wang et al., 2001; Zhao and Zhou, 2006; Zhou et al., 2022). However, these studies have generated inconsistent and even contradictory results (An et al., 2000; Rao et al., 2016; Zhao et al., 2009; Zhou et al., 2016). These discrepancies can be attributed in part to the scarcity of studies in southern China. Previous studies have investigated Holocene hydrological changes in southern China using geological data obtained predominantly from terrestrial records and deep-sea sediments (Hu et al., 2012; Jia et al., 2015; Li et al., 2021; Yu et al., 2021; Zhong et al., 2017b). In comparison, high-resolution records from continental-shelf sediments in the northern South China Sea (SCS) are relatively scarce. Continental shelf settings are characterised by relatively stable depositional environments and high sedimentation rates. Sediment cores from continental shelves should therefore provide the opportunity to investigate the historical evolution of regional precipitation. In this study, we report high-resolution geochemical and grain-size records from marine sediments of the continental shelf of the northern SCS. The main objective was to establish the history of hydroclimatic change in southern China and identify the relevant forcing mechanisms.

2 Materials and methods

Core HKA-1 (20.96°N, 110.74°E; 2.6 m in length) was retrieved from a water depth of 20 m on the continental shelf off eastern Leizhou Peninsula using a gravity corer (Fig. 1). The

Foundation item: The National Natural Science Foundation of China under contract No. 42001078; the College Student Innovation and Training Project of Guangdong Ocean University under contract No. S20211056601; the Guangdong Natural Science Foundation of China under contract No. 2021A1515011157; the Innovative Team Project of Guangdong Universities under contract No. 2019KCXTF021; the First-class Discipline Plan of Guangdong Province under contract Nos 080503032101 and 231420003; the Marine Science Research Team Project of Guangdong Ocean University under contract No. 002026002004.
*Corresponding author, E-mail: fjchen@gdou.edu.cn

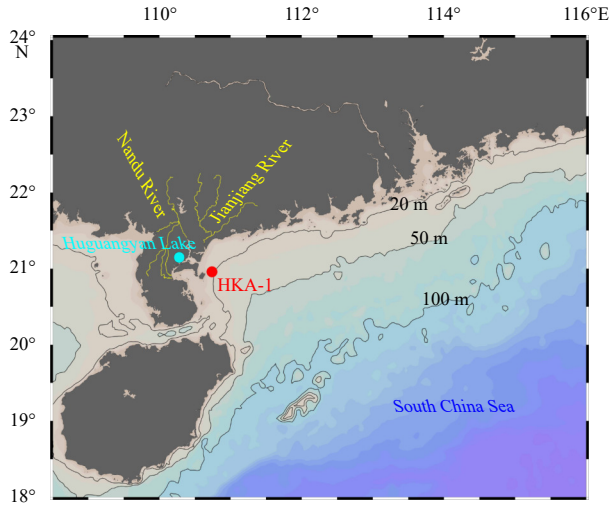

Fig. 1. Map of the study area showing the location of Core HKA-1.

study area is strongly influenced by the monsoon climate, which shows very strong seasonality. The modern annual mean temperature of the study area is about 23℃, and the annual mean precipitation is around 1 600 mm, with over 90% of rainfall occurring between April and October. Most of the precipitation is caused by convection. Convectional precipitation is heavy but of short duration and highly localised.

The chronology of Core HKA-1 was established using five Asian summer monsoon (AMS) ^{14}C dates from well-preserved shell samples (Table 1; Fig. 2). AMS ^{14}C dates were measured at the BETA Laboratory, United States. All radiocarbon dates were calibrated to calendar ages using the Calib 8.1.0 software with the marine20 program (Reimer et al., 2020). An age model of Core HKA-1 was established using the BACON software package (Blaauw and Christen, 2011).

Bulk sediment samples were freeze-dried and ground to #200 mesh, then heated at 650℃ for 4 h to remove organic matter. The samples were digested in an HNO_3 + HF acid mixture, and the resultant solutions were used for analyses of major- and trace-element contents. Major-element contents (e.g., Al_2O_3, TiO_2, Fe_2O_3, and MnO) were measured on a Varian 720 ES Inductively Coupled Plasma–Atomic Emission Spectrometer (ICP–AES at the Qingdao Sparta Analysis & Testing Co.,Ltd, China). Trace-element contents (e.g., La, Th, Sc, Rb, and Sr) were measured on a Varian 820 Inductively Coupled Plasma–Mass Spectrometer (ICP–MS at the Qingdao Sparta Analysis & Testing Co.,Ltd, China). Precision and accuracy were monitored by analysing Chinese certified reference standards BHVO-2, BCR-2, GBW07314, GBW07315, and GBW07316, yielding values that were generally within ±10% (relative standard deviation) of the certified values. The chemical index of alteration (CIA), defined as $Al_2O_3/(Al_2O_3 + CaO + Na_2O + K_2O) \times 100$, using molecular pro-

Table 1. Details and Asian summer monsoon ^{14}C dates of the 5 shell samples from Core HKA-1

Sample code	Depth/cm	Material	Conventional age/(a BP)	Error (2σ)	Calibrated age/(a BP)	Error (2σ)
HKA-1-17	17	shell	5 960	56	6 336	181
HKA-1-26	26	shell	6 020	56	6 393.5	183.5
HKA-1-35	35	shell	6 280	56	6 675	200
HKA-1-96	96	shell	7 570	56	7 992	173
HKA-1-189	189	shell	8 280	56	8 789.5	207.5

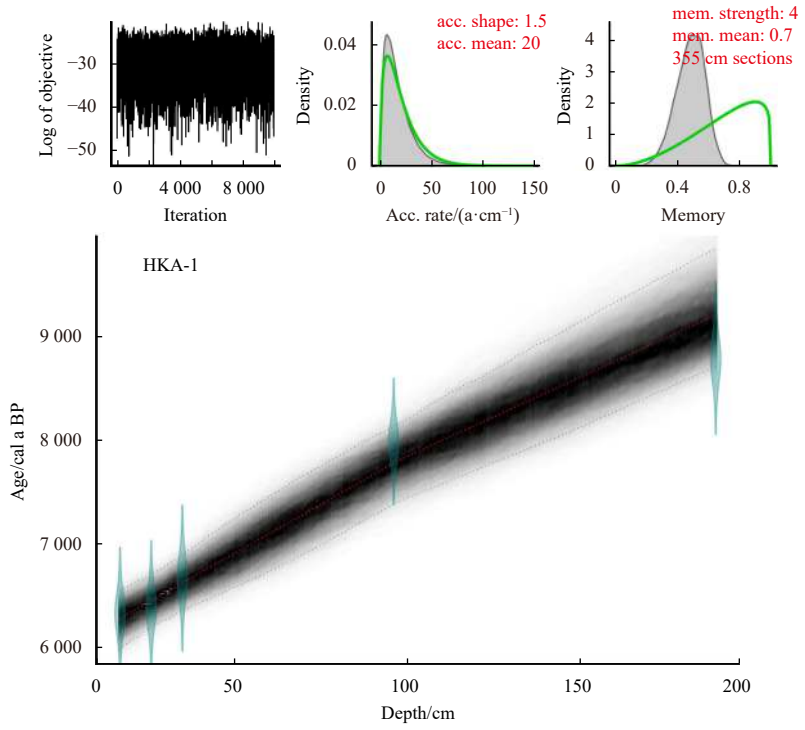

Fig. 2. Bayesian age-depth model for Core HKA-1. acc.: accumulative; mem.: memory.

portions, has been widely used to indicate changes in chemical weathering intensity (Nesbitt and Young, 1982). In the present study, it was difficult to evaluate the CaO content of the silicate fraction. The CIA was therefore calculated using the following formula, which excludes CaO: molar $Al_2O_3/(Al_2O_3 + Na_2O + K_2O) \times 100$ (Arnaud et al., 2012; Li et al., 2017; Liu et al., 2014a). This amendment does not substantially affect the results because only relative variations in chemical weathering are considered (Arnaud et al., 2012).

For grain-size analysis, samples were pretreated with 10% H_2O_2 followed by 10% HCl to remove organic matter and carbonates, respectively. Samples were then rinsed with deionised water and dispersed with 10 mL of 0.05 mol/L $(NaPO_3)_6$ using an ultrasonic vibrator for 10 min. Grain-size distributions were measured using a Malvern 3000 laser-diffraction instrument.

3 Results

The analysed sediments have a rather uniform lithology, with no distinct vestiges or trace fossils of marine benthos (Fig. 3). The five AMS ^{14}C ages are in correct chronological order through the core. These observations suggest that bioturbation mixing is insignificant. Previous studies have demonstrated that bioturbation may have little impact on paleorecords derived from sediments with high rates of deposition (Barker et al., 2007; Higginson et al., 2004; Verschuren, 1999). Given the high sedimentation rate in Core HKA-1 (mean sedimentation rate of ~6 mm/a), we consider that bioturbation had a minor influence on the continuity of the record. The uppermost 1.9 m of Core HKA-1 covers the interval corresponding to 9 200–6 200 cal a BP (Fig. 2). The age of the top of the Core HKA-1 is about 6 200 cal a BP according to the three closest age controls. The absence of sediment over the last 6 000 a at the top of the core may have been caused by modern shipping, navigation projects, and infrastructure, as the studied core was obtained from a location near a major sea route. In addition, no shell material was found for dating below 1.9 m in the core. Therefore, we focus on the paleoclimatic record contained in the uppermost 1.9 m of the core, which covers the period 9 200–6 200 cal a BP.

The variations in CIA, Al/Ti, Al/K, and Rb/Sr, grain-size parameters, and contents of Al, Ti, and Fe show similar temporal patterns (Fig. 4). The variations in these proxies of environmental conditions can be divided into four stages. For the interval 9 200–7 600 cal a BP, values of CIA, Al/Ti, Al/K, and Rb/Sr, and contents of Al, Ti, and Fe are relatively high and display high-frequency fluctuations. The clay and silt fractions exhibit relatively high values, whereas the sand fraction displays relatively low values with high-frequency fluctuations. For the interval

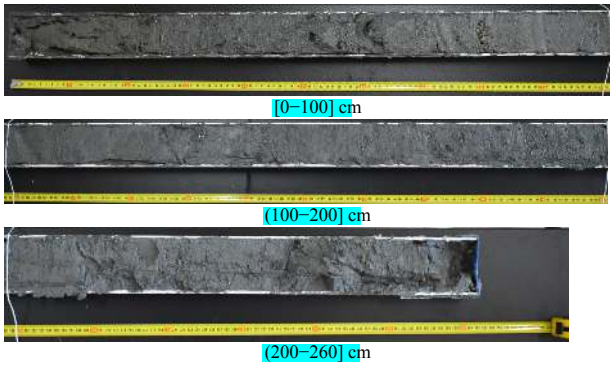

Fig. 3. The photograph of Core HKA-1.

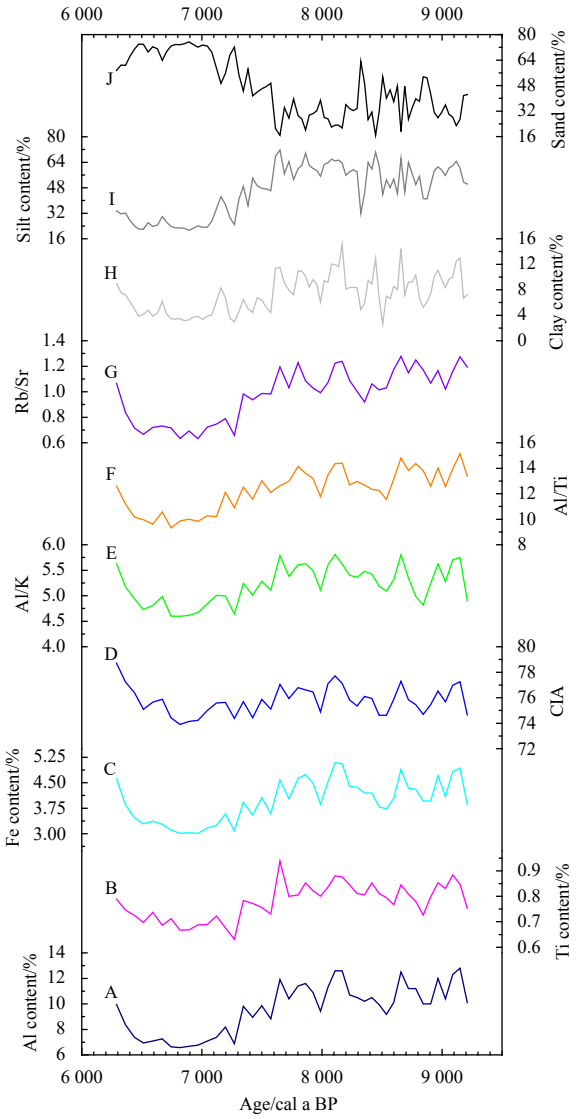

Fig. 4. Temporal variations in multiple proxies in Core HKA-1.

7 600–7 200 cal a BP, all measured proxies show an abrupt shift. Values of CIA, Al/Ti, Al/K, and Rb/Sr, and contents of Al, Ti, and Fe all display a sharp decrease. The clay and silt fractions exhibit a clear decreasing trend, but the sand fraction exhibits a sharp increase. For the interval 7 200–6 500 cal a BP, values of CIA, Al/Ti, Al/K, and Rb/Sr, and contents of Al, Ti, and Fe show relatively low values and remain fairly uniform. The clay and silt fractions show relatively low values, and the sand fraction displays high values with small-amplitude fluctuations. For the interval 6 500–6 200 cal a BP, values of CIA, Al/Ti, Al/K, and Rb/Sr, and contents of Al, Ti, and Fe show clear increasing trends. The clay and silt fractions exhibit an overall increase, and the sand fraction displays an overall decrease.

4 Discussion

4.1 *Paleoclimatic significance of the measured environmental proxies*

Chemical weathering can modify the chemical components of continental surfaces, and components in sediments are composed of the products of chemical weathering. Thus, selected elemental contents and ratios in detrital sediments can be used as

indicators of chemical weathering to trace climatic changes in the source region(s) of the sediments (Kronberg et al., 1986; Liu et al., 2011; Nesbitt and Young, 1982; Wei et al., 2004, 2006). Elemental ratios are widely considered to indicate the intensity of chemical weathering, as they reflect the differing behaviours of different elements during chemical weathering. Ti and K tend to be enriched in weathering products after a moderate degree of chemical weathering, but depleted after extreme chemical weathering (Nesbitt et al., 1980; Condie et al., 1995), whereas Al tends to become enriched in weathering products during chemical weathering. Thus, Al/Ti and Al/K ratios can be used to trace the intensity of chemical weathering, with higher values indicating stronger chemical weathering. Sr is chemically mobile and easily leached from the parent rock, whereas Rb is chemically immobile and tends to become enriched in weathering products during chemical weathering (Brass, 1975). Thus, Rb/Sr ratios are a good indicator of the degree of chemical weathering. Ratios of Al/Ti, Al/K, and Rb/Sr have been successfully used to indicate the intensity of chemical weathering in continental-shelf and deep-sea sedimentary records of the northern SCS (Clift et al., 2014; Hu et al., 2012; Huang et al., 2021; Li et al., 2003; Wei et al., 2006), further supporting the rationale for using Al/Ti, Al/K, and Rb/Sr ratios as indicators of chemical weathering intensity in the present study. In Core HKA-1, values of Al/Ti, Al/K, and Rb/Sr exhibit similar variation patterns to those of CIA values (Figs. 4D and E) and are interpreted as reliably reflecting variations in chemical weathering intensity. The climate is generally considered to be the main control on the degree of chemical weathering under given environmental conditions (White and Blum, 1995), with warm and humid conditions favouring intense chemical weathering. The study area is strongly influenced by the ASM (Jia et al., 2015; Wang et al., 2016). Consequently, values of CIA, Al/Ti, Al/K, and Rb/Sr in Core HKA-1, which are indicators of chemical weathering intensity, can be used to track variations in the intensity of the summer monsoon.

In marine sediments, Al, Ti, and Fe are derived primarily from terrigenous detrital materials, and these elemental contents have been widely used to indicate variations in the influx of terrigenous materials into the marine depositional environment (Latimer and Filippelli, 2001; Ishfaq et al., 2013; Revel et al., 2010). Moreover, our previous published studies have confirmed that contents of Al, Ti, and Fe in continental-shelf sediments from the northern SCS can be successfully used to trace changes in terrigenous material influx (Huang et al., 2019, 2021), supporting the rationale for using Al, Ti, and Fe variations in Core HKA-1 as tracers of terrigenous influx. Previous studies in southern China have confirmed that monsoonal precipitation is the dominant control on the intensity of continental erosion, with higher monsoonal precipitation generating a greater influx of terrigenous materials (Clift et al., 2014; Hu et al., 2012; Wan et al., 2015). In Core HKA-1, contents of Al, Ti, and Fe show similar temporal patterns to those of CIA values and Al/Ti, Al/K, and Rb/Sr ratios. We therefore conclude that strong monsoonal precipitation favours chemical weathering and thus generates greater volumes of terrigenous detrital materials.

The grain-size distribution of marine sediments provides useful information about paleoenvironmental conditions (Boulay et al., 2007; Hu et al., 2012; Huang et al., 2011; Liu et al., 2016). Warm and humid monsoonal conditions favour intense chemical weathering and generate large volumes of fine particles (Dinakaran and Krishnayya, 2011; Hu et al., 2012; Liu and Deng, 2014). The relative proportion of clay-sized particles in marine sediments from the SCS has been used as an indicator of the amount of terrigenous material input generated by continental erosion caused by summer monsoonal precipitation (Hu et al., 2012; Wang et al., 1999a, b). In general, higher monsoonal precipitation generates greater fluvial discharges and, eventually, larger volumes of clay-sized particles in the marine depositional environment. The clay content (fraction) in Core HKA-1 shows similar patterns of variation to those of Al/K ratios and contents of Al, Ti, and Fe (Fig. 4), which are considered to indicate variations in chemical weathering intensity and the amount of terrigenous sediment influx, respectively. Therefore, we can infer that higher monsoonal precipitation would trigger stronger chemical weathering and a greater influx of terrigenous material, thereby generating a higher proportion of clay in the continental shelf sediments.

Core HKA-1 was collected from the northwestern shelf of the SCS (Fig. 1). The terrigenous detrital sediments on the shelf of the SCS are derived predominantly from the inputs of rivers in the surrounding area. The Jianjiang River and Nandu River are the two main rivers in the study area and discharge terrestrially sourced sediments into the sea (Fig. 1). The sand content of these two rivers is relatively high at ~0.38 kg/m^3 (Wang, 2007). Sediment samples from these rivers are consistent with the sediment types in Core HKA-1 (Gao et al., 2015), suggesting a common provenance. Grain-size trend analysis suggests that the net sediment transport vectors offshore of the Jianjiang and Nandu rivers are towards the southeast (Liu et al., 2014b; Xu et al., 2014). The net sediment transport pathways illustrate a potential convergence of terrigenous-derived surficial sediments to the location of Core HKA-1. In addition, studies of heavy mineral geochemistry and U–Pb ages of detrital zircons from sediments on the northwestern shelf of the SCS have suggested that sandy sediments on the northwestern shelf of the SCS were supplied mostly by the Jianjiang River (Li et al., 2015; Zhong et al., 2017a). It is therefore probable that the sediments of Core HKA-1 originated mainly from sediment discharge of the Jianjiang River and Nandu River. As over 90% of modern rainfall occurs during the wet season (April to October), summer monsoonal precipitation plays a key role in transporting sediments from the Jianjiang River and Nandu River to the western shelf of the SCS. In summary, monsoon precipitation seems to be the primary control of the levels of chemical weathering and continental erosion in southern China. Thus, higher monsoonal precipitation would generate stronger chemical weathering, higher rates of physical erosion and a greater fluvial sediment input into the SCS area, subsequently supplying a greater proportion of clay into sediments of Core HKA-1.

4.2 *Climate change during 9 200–6 200 cal a BP*

Multi-proxy records from core HKA-1 show similar trands and wide fluctuations for the period 9 200–6 200 cal a BP (Fig. 4). These high-resolution records allow us to investigate paleoclimatic and hydrological variations during this interval.

Given that Core HKA-1 is located close to the coast (Fig. 1), fluvial sediment discharge and shelf sediment deposition have probably been influenced by changes in the location of the shoreline. Thus, it is essential to consider the influence of relative sea-level change on the proxies measured for Core HKA-1. During the interval 9 200–7 600 cal a BP, following a stage of sea level rise (Fig. 5G; Zong, 2004), a decreasing trend of terrigenous sediment influx into the shelf area would have been expected. However, contents of Al, Ti, and Fe for this interval remain relatively high and uniform and do not show any clear trend, suggesting that the terrigenous material influx was consistent throu-

ghout this period, in turn implying that variation in sea level was not a dominant control on terrigenous sediment influx. The ASM inferred from various records in southern China was extremely strong for the period 9 200 cal a BP to 7 600 cal a BP (Huang et al., 2016; Duan et al., 2014; Dykoski et al., 2005; Zhong et al., 2010). The relatively high influx of terrigenous sediment can therefore be attributed to the strong ASM during this interval. During the period 7 600–7 200 cal a BP, sea level rose rapidly (Fig. 5G; Zong, 2004), and the distance between the site of Core HKA-1 and the shoreline increased. During this interval, Al, Ti, and Fe show a sharp decrease and clay content exhibits a marked decrease. This correspondence of sea level change and proxies suggests that the abrupt decrease in sediment discharge was caused by the rapid rise in sea level. In addition, previous studies have detected an abrupt decline in ASM intensity during 7 600–7 200 cal a BP (Dykoski et al., 2005; Zhang et al., 2011). We therefore conclude that sea level change and the intensity of the ASM controlled collectively changes in terrigenous sediment influx during 7 600–7 200 cal a BP. Sea level was constant from 7 200 cal a BP to 6 200 cal a BP (Fig. 5G; Zong, 2004), whereas the sediment discharge

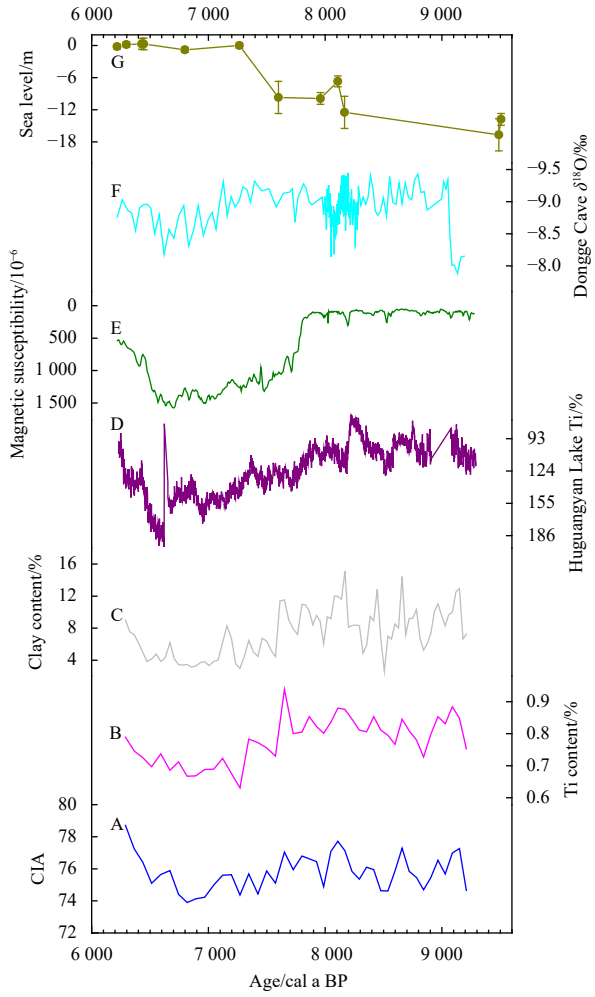

Fig. 5. Comparison between related records: CIA values in Core HKA-1 (A); Ti contents in Core HKA-1 (B); clay contents in Core HKA-1 (C); Ti contents from Huguangyan Lake (Yancheva et al., 2007) (D); magnetic susceptibility from Huguangyan Lake (Yancheva et al., 2007) (E); stalagmite δ^{18}O record from Dongge Cave (Dykoski et al., 2005) (F); sea level change in South China (Zong, 2004) (G).

inferred from our data exhibits wide fluctuations. These non-corresponding patterns suggest that variations in sediment discharge during the interval 7 200–6 200 cal a BP were not related to sea level.

For the interval of core corresponding to 9 200 cal a BP to 7 600 cal a BP, values of CIA, Al/Ti, Al/K, and Rb/Sr are high and show high-frequency fluctuations, indicating intensive chemical weathering, likely a result of an intense ASM. Similarly, high proportions of clay and contents of Al, Ti, and Fe reflect a strong influx of terrigenous material, suggesting high monsoonal precipitation. The negative excursion in δ^{18}O values recorded from Dongge Cave during this period indicates a strong summer monsoon (Fig. 5F; Dykoski et al., 2005). The prevalence of a strong summer monsoon during 9 200 cal a BP to 7 600 cal a BP has also been inferred from chemical weathering records from ODP Site 1144 and Core KNG5 in the northern SCS (Hu et al., 2012; Huang et al., 2016). An intense summer monsoon during this period would have favoured intense chemical weathering and generated large amounts of terrigenous clastic material to be discharged offshore, eventually leading to a higher proportion of clay in the sediments of Core HKA-1.

For the interval 7 600–7 200 cal a BP, the intensity of chemical weathering decreases sharply, as indicated by the profiles of CIA, Al/Ti, Al/K, and Rb/Sr for Core HKA-1. The terrigenous sediment influx is inferred to have decreased rapidly during this period, as indicated by the contents of Al, Ti, and Fe. The clay fraction also shows a marked decrease in this interval. The abrupt shifts in these proxies measured from Core HKA-1 seem to indicate a rapid deterioration in climate, which is ascribed to an abrupt decrease in the intensity of the summer monsoon. Huguangyan Lake is close to Core HKA-1. Contents of Ti and the magnetic properties of sediments from Huguangyan Lake have been interpreted as indicators of the intensity of the winter monsoon (Yancheva et al., 2007). However, Zhou et al. (2007) and Zaarur et al. (2018) argued that sedimentary Ti in Huguangyan Lake would have been derived mainly from catchment erosion rather than aeolian input, and therefore variations in Ti content of sediment should be associated with changes in regional hydrology. Shen et al. (2013) further proposed that Ti supply is controlled by monsoon-dominated vegetation density, with strong monsoonal precipitation causing lower input of Ti into sediment. Several studies have confirmed that the magnetic properties of sediment from Huguangyan Lake do not indicate variations in the intensity of the winter monsoon, as magnetic minerals are derived mainly from eroded pyroclastic material from the catchment (Duan et al., 2014; Wang et al., 2016; Wu et al., 2012). Those studies also proposed that magnetic properties of sediments should be inversely correlated to summer monsoon intensity. Modern process investigation has provided further evidence that magnetic minerals are derived mainly from weathered materials in the catchment rather than aeolian dust input (Zhong et al., 2021). The sedimentary Ti contents and magnetic susceptibility in the studied core exhibit a marked increase in the interval 7 600–7 200 cal a BP (Figs. 5D and E), suggesting an abrupt weakening in the summer monsoon (Yancheva et al., 2007), which coincides with the abrupt climatic shift inferred from the measured proxies of Core HKA-1.

For the interval 7 200 cal a BP to 6 500 cal a BP, values of CIA, Al/Ti, Al/K, and Rb/Sr are relatively low, indicating weak chemical weathering. The low clay content for this interval suggests a low influx of terrigenous material, which is supported by the low contents of Al, Ti, and Fe. The relatively low values of these proxies in Core HKA-1 for 7 200–6 500 cal a BP are attributed to cold

and dry climatic conditions. Within this period, a weak summer monsoon is indicated by a positive excursion in δ^{18}O values in Dongge Cave (Fig. 5F; Dykoski et al., 2005) and the Ti contents and magnetic susceptibility of sediments from Huguangyan Lake (Figs. 5D and E; Yancheva et al., 2007). Such climatic conditions would reduce the intensity of chemical weathering and generate less terrigenous clastic material, thereby leading to a lower proportion of clay particles in sediments of Core HKA-1.

For the interval 6 500–6 200 cal a BP, values of CIA, Al/Ti, Al/K and Rb/Sr show an overall increasing trend, indicating enhanced chemical weathering. The influx of terrigenous sediment also increased during this period, as inferred from the clay fraction and contents of Al, Ti and Fe. Values of δ^{18}O from Dongge Cave exhibit a progressively more negative excursion during this period, implying an enhancing summer monsoon (Fig. 5F; Dykoski et al., 2005). Likewise, sedimentary Ti contents and the magnetic susceptibility of deposits in Huguangyan Lake show an overall increase, consistent with increasing monsoonal precipitation (Figs. 5D and E; Yancheva et al., 2007). These various lines of evidence point towards a stronger summer monsoon during this period.

4.3 *Hydrological anomaly during 7 600–6 500 cal a BP*

During the period 7 600–6 500 cal a BP, relatively low values of CIA, Al/Ti, Al/K, and Rb/Sr, and low contents of Al, Ti, and Fe, with correspondingly low clay contents, indicate less intense chemical weathering and a weak influx of terrigenous material, reflecting a dry period. Values of δ^{18}O recorded from Dongge Cave show a positive excursion, suggesting an arid climate during this period (Fig. 5F; Dykoski et al., 2005). Dry climatic conditions are also inferred from the Ti contents and magnetic susceptibility properties of sediments from Huguangyan Lake (Figs. 5D and E; Yancheva et al., 2007). The inferred dry conditions during this period are supported by magnetic data of stalagmites from Heshang Cave in the Jianghan Basin (Zhu et al., 2017), grain-size parameters of sediments from Tengchong Qinghai Lake (Zhang et al., 2017), and low water levels at Lake Chenghai (Xu et al., 2020). Taken together, these data in southern China indicate dry climatic conditions during 7 600–6 500 cal a BP.

Within dating uncertainties, the dry climatic conditions between 7 600 cal a BP and 6 500 cal a BP recorded in Core HKA-1 are broadly consistent with the east–west equatorial Pacific thermal gradient (Fig. 6D; Koutavas and Joanides, 2012). This synchroneity suggests a link between hydrological change in southern China and variation in tropical Pacific sea surface temperatures (SSTs). Modern observations suggest that summer rainfall over China is closely related to the thermal state of the tropical Pacific (Chang et al., 2000; Chiang et al., 2015; Ding et al., 2008; Wang et al., 2013). A temperature anomaly in the tropical Pacific would affect rainfall over southern China by modulating the intensity and location of the West Pacific subtropical high (WPSH) (Hu, 1997; Zhou et al., 2009). A warmer (colder) SST in the tropical western Pacific would generate stronger (weaker) convective activity in the tropical Indian Ocean and tropical western Pacific, and produce a strengthening and southwestward (weakening and northeastward) displacement of the WPSH, thereby causing less (more) rainfall over southern China (Huang and Sun, 1992). The changes in multiple proxies measured for Core HKA-1 correspond to variation in the east–west equatorial Pacific thermal gradient during the interval 7 600–6 500 cal a BP. Using TraCE-21ka simulations, Liu et al. (2014c) demonstrated that the WPSH gradually became displaced westward during this period. It would therefore appear that the coupled variation in tropical Pacific SST and the WPSH potentially modulate moisture variations over southern China. During the period 7 600–6 500 cal a BP, convective activity over the tropical western Pacific was enhanced owing to an increased east–west equatorial Pacific thermal gradient, which favoured the intensification and southwestward displacement of the WPSH, eventually causing less rainfall in southern China.

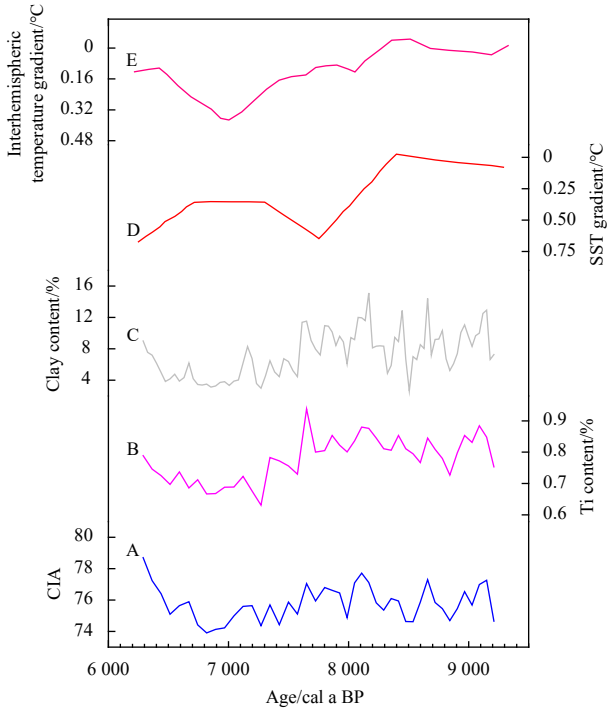

Fig. 6. Comparison between various paleoclimate records: CIA values in Core HKA-1 (A); Ti contents in Core HKA-1 (B); clay contents in Core HKA-1 (C); tropical Pacific sea surface temperature (SST) gradient (Koutavas and Joanides, 2012) (D); Northern-Southern hemisphere temperature gradients (McGee et al., 2014) (E).

In addition, temperature gradients between the northern and southern hemispheres potentially mediate the intensity and location of the WPSH and subsequently influence hydrological change (McGee et al., 2014). In terms of overall trends, the indicators of chemical weathering and terrigenous sediment influx measured for Core HKA-1 show a similar pattern to variations in interhemispheric temperature gradients (Fig. 6E; McGee et al., 2014). During the interval 7 600–6 500 cal a BP, dry climatic conditions were recorded in Core HKA-1, and interhemispheric temperature gradients were large, consistent with a strengthening and southwestward displacement of the WPSH (Liu et al., 2014c). These results suggest a link and interaction between hydrological change in southern China, tropical Pacific SST, and the WPSH.

5 Conclusions

This study has established high-resolution geochemical and grain-size records for the interval 9 200–6 200 cal a BP in Core HKA-1 obtained from coastal shelf sediments of the northern SCS. Results suggest that the geochemical and grain-size variables measured in the core can be used as environmental proxies and are sensitive to regional climatic and hydrological conditions. During the interval 9 200–7 600 cal a BP, multiple proxies reveal warm and humid climate conditions, which are inferred to have been generated by strong monsoonal precipitation. The

subsequent stage, from 7 600 cal a BP to 7 200 cal a BP, was characterised by abrupt decreases in terrigenous sediment influx and the intensity of chemical weathering in the continental sedimentary source region, indicating the combined influence of sea level rise and a strong ASM. During the period 7 200–6 500 cal a BP, cold and dry climatic conditions are recorded, probably resulting from a weak ASM. During the interval 6 500–6 200 cal a BP, the enhancement of continental chemical weathering and terrigenous sediment influx is attributed to increasing monsoonal precipitation. The measured proxies show a prominent hydrological anomaly for the period 7 600–6 500 cal a BP, coincident with a dramatic decrease in monsoonal precipitation. This abrupt hydrological event was synchronous with tropical Pacific SST and interhemispheric temperature gradients. We therefore conclude that the zonal Pacific and interhemispheric temperature gradients influenced moisture variations in southern China by modulating the intensity and location of the WPSH.

References

An Zhisheng, Porter S C, Kutzbach J E, et al. 2000. Asynchronous Holocene optimum of the East Asian monsoon. Quaternary Science Reviews, 19(8): 743–762, doi: 10.1016/S0277-3791(99)00031-1

Arnaud F, Révillon S, Debret M, et al. 2012. Lake Bourget regional erosion patterns reconstruction reveals Holocene NW European Alps soil evolution and paleohydrology. Quaternary Science Reviews, 51: 81–92, doi: 10.1016/J.QUASCIREV.2012.07.025

Barker S, Broecker W, Clark E, et al. 2007. Radiocarbon age offsets of foraminifera resulting from differential dissolution and fragmentation within the sedimentary bioturbated zone. Paleoceanography, 22(2): PA2205, doi: 10.1029/2006PA001354

Blaauw M, Christen J A. 2011. Flexible paleoclimate age-depth models using an autoregressive gamma process. Bayesian Analysis, 6(3): 457–474, doi: 10.1214/11-BA618

Boulay S, Colin C, Trentesaux A, et al. 2007. Sedimentary responses to the Pleistocene climatic variations recorded in the South China Sea. Quaternary Research, 68(1): 162–172, doi: 10.1016/J.YQRES.2007.03.004

Brass G W. 1975. The effect of weathering on the distribution of strontium isotopes in weathering profiles. Geochimica et Cosmochimica Acta, 39(12): 1647–1653, doi: 10.1016/0016-7037(75)90086-1

Chang C P, Zhang Yongsheng, Li T. 2000. Interannual and interdecadal variations of the East Asian summer monsoon and tropical Pacific SSTs. Part II: Meridional structure of the monsoon. Journal of Climate, 13(24): 4326–4340, doi: 10.1175/1520-0442(2000)013<4326:IAIVOT>2.0.CO;2

Chiang J C H, Fung I Y, Wu Chihua, et al. 2015. Role of seasonal transitions and westerly jets in East Asian paleoclimate. Quaternary Science Reviews, 108: 111–129, doi: 10.1016/J.QUASCIREV.2014.11.009

Clift P D, Wan Shiming, Blusztajn J. 2014. Reconstructing chemical weathering, physical erosion and monsoon intensity since 25 Ma in the northern South China Sea: a review of competing proxies. Earth-Science Reviews, 130: 86–102, doi: 10.1016/J.EARSCIREV.2014.01.002

Condie K C, Dengate J, Cullers R L. 1995. Behavior of rare earth elements in a paleoweathering profile on granodiorite in the Front Range, Colorado, USA. Geochimica et Cosmochimica Acta, 59(2): 279–294, doi: 10.1016/0016-7037(94)00280-Y

Dinakaran J, Krishnayya N S R. 2011. Variations in total organic carbon and grain size distribution in ephemeral river sediments in western India. International Journal of Sediment Research, 26(2): 239–246, doi: 10.1016/S1001-6279(11)60090-5

Ding Yihui, Wang Zunya, Sun Ying. 2008. Inter-decadal variation of the summer precipitation in East China and its association with decreasing Asian summer monsoon. Part I: Observed evidences. International Journal of Climatology, 28(9): 1139–1161, doi: 10.1002/JOC.1615

Duan Zongqi, Liu Qingsong, Yang Xiaoqiang, et al. 2014. Magnetism of the Huguangyan Maar Lake sediments, Southeast China and its paleoenvironmental implications. Palaeogeography, Palaeoclimatology, Palaeoecology, 395: 158–167, doi: 10.1016/J.PALAEO.2013.12.033

Dykoski C A, Edwards R L, Cheng Hai, et al. 2005. A high-resolution, absolute-dated Holocene and deglacial Asian monsoon record from Dongge Cave, China. Earth and Planetary Science Letters, 233(1–2): 71–86, doi: 10.1016/J.EPSL.2005.01.036

Gao Shu, Liu Yunling, Yang Yang, et al. 2015. Evolution status of the distal mud deposit associated with the Pearl River, northern South China Sea continental shelf. Journal of Asian Earth Sciences, 114: 562–573, doi: 10.1016/j.jseaes.2015.07.024

Higginson M J, Altabet M A, Murray D W, et al. 2004. Geochemical evidence for abrupt changes in relative strength of the Arabian monsoons during a stadial/interstadial climate transition. Geochimica et Cosmochimica Acta, 68(19): 3807–3826, doi: 10.1016/j.gca.2004.03.015

Hu Zengzhen. 1997. Interdecadal variability of summer climate over East Asia and its association with 500 hPa height and global sea surface temperature. Journal of Geophysical Research: Atmospheres, 102(D16): 19403–19412, doi: 10.1029/97JD01052

Hu Dengke, Böning P, Köhler C M, et al. 2012. Deep sea records of the continental weathering and erosion response to East Asian monsoon intensification since 14 ka in the South China Sea. Chemical Geology, 326–327: 1–18, doi: 10.1016/J.CHEMGEO.2012.07.024

Huang Chao, Kong Deming, Chen Fajin, et al. 2021. Multi-proxy reconstructions of climate change and human impacts over the past 7 000 years from an archive of continental shelf sediments off eastern Hainan Island, China. Frontiers in Earth Science, 9: 663634, doi: 10.3389/FEART.2021.663634

Huang Jie, Li Anchun, Wan Shiming. 2011. Sensitive grain-size records of Holocene East Asian summer monsoon in sediments of northern South China Sea slope. Quaternary Research, 75(3): 734–744, doi: 10.1016/J.YQRES.2011.03.002

Huang Ronghui, Sun Fengying. 1992. Impacts of the tropical western pacific on the East Asian summer monsoon. Journal of the Meteorological Society of Japan. Ser. II, 70(1B): 243–256, doi: 10.2151/JMSJ1965.70.1B_243

Huang Jie, Wan Shiming, Xiong Zhifang, et al. 2016. Geochemical records of Taiwan-sourced sediments in the South China Sea linked to Holocene climate changes. Palaeogeography, Palaeoclimatology, Palaeoecology, 441: 871–881, doi: 10.1016/J.PALAEO.2015.10.036

Huang Chao, Zeng Ti, Ye Feng, et al. 2019. Solar-forcing-induced spatial synchronisation of the East Asian summer monsoon on centennial timescales. Palaeogeography, Palaeoclimatology, Palaeoecology, 514: 536–549, doi: 10.1016/J.PALAEO.2018.11.002

IPCC. 2021. The physical science basis. Contribution of working group I to the sixth assessment report of the intergovernmental panel on climate change. Cambridge, United Kingdom and New York, NY: Cambridge University Press, 2391. doi: 10.1017/9781009157896

Ishfaq A M, Pattan J N, Matta V M, et al. 2013. Variation of paleo-productivity and terrigenous input in the Eastern Arabian Sea during the past 100 ka. Journal of the Geological Society of India, 81(5): 647–654, doi: 10.1007/S12594-013-0086-7

Jia Guodong, Bai Yang, Yang Xiaoqiang, et al. 2015. Biogeochemical evidence of Holocene East Asian summer and winter monsoon variability from a tropical maar lake in southern China. Quaternary Science Reviews, 111: 51–61, doi: 10.1016/J.QUASCIREV.2015.01.002

Koutavas A, Joanides S. 2012. El Niño–southern oscillation extrema in the Holocene and last glacial maximum. Paleoceanography, 27(4): PA4208, doi: 10.1029/2012PA002378

Kronberg B I, Nesbitt H W, Lam W W. 1986. Upper Pleistocene Amazon deep-sea fan muds reflect intense chemical weather-

ing of their mountainous source lands. Chemical Geology, 54(3–4): 283–294, doi: 10.1016/0009-2541(86)90143-9
Latimer J C, Filippelli G M. 2001. Terrigenous input and paleoproductivity in the Southern Ocean. Paleoceanography, 16(6): 627–643, doi: 10.1029/2000PA000586
Li Pingyuan, Li Mingkun, Gan Huayang, et al. 2021. A preliminary study on sediment records of possible typhoon in the northern South China Sea during the past 6 500 years. The Holocene, 31(7): 1221–1228, doi: 10.1177/09596836211003229
Li Jingrui, Liu Shengfa, Feng Xiuli, et al. 2017. Major and trace element geochemistry of the mid-Bay of Bengal surface sediments: implications for provenance. Acta Oceanologica Sinica, 36(3): 82–90, doi: 10.1007/s13131-017-1041-z
Li Xianhua, Wei Gangjian, Shao Lei, et al. 2003. Geochemical and Nd isotopic variations in sediments of the South China Sea: a response to Cenozoic tectonism in SE Asia. Earth and Planetary Science Letters, 211(3–4): 207–220, doi: 10.1016/S0012-821X(03)00229-2
Li Gang, Yan Wen, Zhong Lifeng, et al. 2015. Provenance of heavy mineral deposits on the northwestern shelf of the South China Sea, evidence from single-mineral chemistry. Marine Geology, 363: 112–124, doi: 10.1016/j.margeo.2015.01.015
Liu Jianbao, Chen Jianhui, Selvaraj K, et al. 2014a. Chemical weathering over the last 1 200 years recorded in the sediments of Gonghai Lake, Lvliang Mountains, North China: a high-resolution proxy of past climate. Boreas, 43(4): 914–923, doi: 10.1111/BOR.12072
Liu Caicai, Deng Chenglong. 2014. The effect of weathering on the grain-size distribution of red soils in south-eastern China and its climatic implications. Journal of Asian Earth Sciences, 94: 94–104, doi: 10.1016/J.JSEAES.2014.08.027
Liu Yunling, Gao Shu, Wang Yaping, et al. 2014b. Distal mud deposits associated with the Pearl River over the northwestern continental shelf of the South China Sea. Marine Geology, 347: 43–57, doi: 10.1016/j.margeo.2013.10.012
Liu Zhengyu, Lu Zhengyao, Wen Xinyu, et al. 2014c. Evolution and forcing mechanisms of El Niño over the past 21, 000 years. Nature, 515(7528): 550–553, doi: 10.1038/NATURE13963
Liu Shengfa, Shi Xuefa, Liu Yanguang, et al. 2011. Environmental record from the mud area on the inner continental shelf of the East China Sea since the mid-Holocene. Acta Oceanologica Sinica, 30(4): 43–52, doi: 10.1007/s13131-011-0132-5
Liu Jianguo, Xiang Rong, Kao S J, et al. 2016. Sedimentary responses to sea-level rise and Kuroshio Current intrusion since the Last Glacial Maximum: Grain size and clay mineral evidence from the northern South China Sea slope. Palaeogeography, Palaeoclimatology, Palaeoecology, 450: 111–121, doi: 10.1016/J.PALAEO.2016.03.002
Lu Jiayi, Yang Huan, Griffiths M L, et al. 2021. Asian monsoon evolution linked to Pacific temperature gradients since the Late Miocene. Earth and Planetary Science Letters, 563: 116882, doi: 10.1016/J.EPSL.2021.116882
McGee D, Donohoe A, Marshall J, et al. 2014. Changes in ITCZ location and cross-equatorial heat transport at the Last Glacial Maximum, Heinrich Stadial 1, and the mid-Holocene. Earth and Planetary Science Letters, 390: 69–79, doi: 10.1016/J.EPSL.2013.12.043
Nesbitt H W, Markovics G, Price R C. 1980. Chemical processes affecting alkalis and alkaline earths during continental weathering. Geochimica et Cosmochimica Acta, 44(11): 1659–1666, doi: 10.1016/0016-7037(80)90218-5
Nesbitt H W, Young G M. 1982. Early Proterozoic climates and plate motions inferred from major element chemistry of lutites. Nature, 299(5885): 715–717, doi: 10.1038/299715A0
Rao Zhiguo, Li Yunxia, Zhang Jiawu, et al. 2016. Investigating the long-term palaeoclimatic controls on the δD and δ^{18}O of precipitation during the Holocene in the Indian and East Asian monsoonal regions. Earth-Science Reviews, 159: 292–305, doi: 10.1016/J.EARSCIREV.2016.06.007
Reimer P J, Austin W E N, Bard E, et al. 2020. The IntCal20 northern hemisphere radiocarbon age calibration curve (0–55 cal kBP). Radiocarbon, 62(4): 725–757, doi: 10.1017/RDC.2020.41
Revel M, Ducassou E, Grousset F E, et al. 2010. 100, 000 Years of African monsoon variability recorded in sediments of the Nile margin. Quaternary Science Reviews, 29(11–12): 1342–1362, doi: 10.1016/J.QUASCIREV.2010.02.006
Shen Ji, Wu Xudong, Zhang Zhaohui, et al. 2013. Ti content in Huguangyan maar lake sediment as a proxy for monsoon-induced vegetation density in the Holocene. Geophysical Research Letters, 40(21): 5757–5763, doi: 10.1002/GRL.50740
Verschuren D. 1999. Sedimentation controls on the preservation and time resolution of climate-proxy records from shallow fluctuating lakes. Quaternary Science Reviews, 18(6): 821–837, doi: 10.1016/S0277-3791(98)00065-1
Wan Shiming, Toucanne S, Clift P D, et al. 2015. Human impact overwhelms long-term climate control of weathering and erosion in southwest China. Geology, 43(5): 439–442, doi: 10.1130/G36570.1
Wang Wenjie. 2007. Study on the Coastal Geomorphological Sedimentation of the South China Sea (in Chinese). Guangzhou: Guangdong Economy Publishing House, 344
Wang Yongjin, Cheng Hai, Edwards R L, et al. 2001. A high-resolution absolute-dated late Pleistocene monsoon record from Hulu Cave, China. Science, 294(5550): 2345–2348, doi: 10.1126/SCIENCE.1064618
Wang Xisheng, Chu Guoqiang, Sheng Mei, et al. 2016. Millennial-scale Asian summer monsoon variations in South China since the last deglaciation. Earth and Planetary Science Letters, 451: 22–30, doi: 10.1016/J.EPSL.2016.07.006
Wang L, Sarnthein M, Erlenkeuser H, et al. 1999a. East Asian monsoon climate during the Late Pleistocene: High-resolution sediment records from the South China Sea. Marine Geology, 156(1–4): 245–284
Wang L, Sarnthein M, Grootes P M, et al. 1999b. Millennial reoccurrence of century-scale abrupt events of East Asian monsoon A possible heat conveyor for the global deglaciation. Paleoceanography, 14(6): 725–731, doi: 10.1029/1999PA900028
Wang Bin, Xiang Baoqiang, Lee J Y. 2013. Subtropical High predictability establishes a promising way for monsoon and tropical storm predictions. Proceedings of the National Academy of Sciences of the United States of America, 110(8): 2718–2722, doi: 10.1073/PNAS.1214626110
Wei Gangjian, Li Xianhua, Liu Ying, et al. 2006. Geochemical record of chemical weathering and monsoon climate change since the early Miocene in the South China Sea. Paleoceanography, 21(4): PA4214, doi: 10.1029/2006PA001300
Wei Gangjian, Liu Ying, Li Xianhua, et al. 2004. Major and trace element variations of the sediments at ODP Site 1144, South China Sea, during the last 230 ka and their paleoclimate implications. Palaeogeography, Palaeoclimatology, Palaeoecology, 212(3–4): 331–342, doi: 10.1016/J.PALAEO.2004.06.011
White A F, Blum A E. 1995. Effects of climate on chemical_ weathering in watersheds. Geochimica et Cosmochimica Acta, 59(9): 1729–1747, doi: 10.1016/0016-7037(95)00078-E
Wu Xudong, Zhang Zhaohui, Xu Xiaomei, et al. 2012. Asian summer monsoonal variations during the Holocene revealed by Huguangyan Maar lake sediment record. Palaeogeography, Palaeoclimatology, Palaeoecology, 323–325: 13–21, doi: 10.1016/J.PALAEO.2012.01.020
Xu Dong, Chu Fengyou, Li Jiabiao, et al. 2014. Transport and deposition of sediment on the shelf off western Guangdong to northeastern Hainan. Journal of Jilin University: Earth Science Edition (in Chinese), 44(3): 905–917, doi: 10.13278/j.cnki.jjuese.201403115
Xu Hai, Goldsmith Y, Lan Jianghu, et al. 2020. Juxtaposition of western Pacific subtropical high on Asian summer monsoon shapes subtropical East Asian precipitation. Geophysical Research Letters, 47(3): e2019GL084705, doi: 10.1029/2019GL084705
Yancheva G, Nowaczyk N R, Mingram J, et al. 2007. Influence of the intertropical convergence zone on the East Asian monsoon. Nature, 445(7123): 74–77, doi: 10.1038/NATURE05431
Yang Song, Min Wen, Higgins R W. 2008. Subseasonal features of the

Asian summer monsoon in the NCEP climate forecast system. Acta Oceanologica Sinica, 27(3): 88–103

Yu Shaohua, Chen Fang, Jing Xia, et al. 2021. Increasing terrigenous pollen input in the late Holocene: Indications of intensive human activity and accelerated delta plain progradation. Marine Geology, 439: 106547, doi: 10.1016/J.MARGEO.2021.106547

Zaarur S, Stein M, Adam O, et al. 2018. Late Quaternary climate in southern China deduced from Sr–Nd isotopes of Huguangyan Maar sediments. Earth and Planetary Science Letters, 496: 10–19, doi: 10.1016/J.EPSL.2018.05.025

Zhang Jiawu, Chen Fahu, Holmes J A, et al. 2011. Holocene monsoon climate documented by oxygen and carbon isotopes from lake sediments and peat bogs in China: a review and synthesis. Quaternary Science Reviews, 30(15–16): 1973–1987, doi: 10.1016/J.QUASCIREV.2011.04.023

Zhang Enlou, Zhao Cheng, Xue Bin, et al. 2017. Millennial-scale hydroclimate variations in southwest China linked to tropical Indian Ocean since the Last Glacial Maximum. Geology, 45(5): 435–438, doi: 10.1130/G38309.1

Zhao Yan, Yu Zicheng, Chen Fahu, et al. 2009. Vegetation response to Holocene climate change in monsoon-influenced region of China. Earth-Science Reviews, 97(1–4): 242–256, doi: 10.1016/J.EARSCIREV.2009.10.007

Zhao Ping, Zhou Xiuji. 2006. Decadal variability of rainfall persistence time and rainbelt shift over eastern China in recent 40 years. Journal of Applied Meteorological Science (in Chinese), 17(5): 548–556

Zhong Lifeng, Li Gang, Yan Wen, et al. 2017a. Using zircon U–Pb ages to constrain the provenance and transport of heavy minerals within the northwestern shelf of the South China Sea. Journal of Asian Earth Sciences, 134: 176–190, doi: 10.1016/j.jseaes.2016.11.019

Zhong Wei, Tang Xiaowen, Shang Shengtan, et al. 2021. Magnetic properties of the surface sediments from the Huguangyan Maar Lake in tropical Southern China and the sediment source identification. Near Surface Geophysics, 19(6): 661–676, doi: 10.1002/NSG.12175

Zhong Wei, Wei Zhiqiang, Chen Yu, et al. 2017b. A 15.4-ka paleoclimate record inferred from $\delta^{13}C$ and $\delta^{15}N$ of organic matter in sediments from the sub-alpine Daping Swamp, western Nanling Mountains, South China. Journal of Paleolimnology, 57(2): 127–139, doi: 10.1007/S10933-016-9935-X

Zhong Wei, Xue Jibin, Zheng Yanming, et al. 2010. Climatic changes since the last deglaciation inferred from a lacustrine sedimentary sequence in the eastern Nanling Mountains, South China. Journal of Quaternary Science, 25(6): 975–984, doi: 10.1002/JQS.1384

Zhou Houyun, Guan Huazheng, Chi Baoquan. 2007. Record of winter monsoon strength. Nature, 450(7168): E10–E11, doi: 10.1038/NATURE06408

Zhou Xin, Sun Liguang, Zhan Tao, et al. 2016. Time-transgressive onset of the Holocene optimum in the East Asian monsoon region. Earth and Planetary Science Letters, 456: 39–46, doi: 10.1016/J.EPSL.2016.09.052

Zhou Tianjun, Yu Rucong, Zhang Jie, et al. 2009. Why the western pacific subtropical high has extended westward since the late 1970s. Journal of Climate, 22(8): 2199–2215, doi: 10.1175/2008JCLI2527.1

Zhou Xin, Zhan Tao, Tu Luyao, et al. 2022. Monthly insolation linked to the time-transgressive nature of the Holocene East Asian monsoon precipitation maximum. Geology, 50(3): 331–335, doi: 10.1130/G49550.1

Zhu Zongmin, Feinberg J M, Xie Shucheng, et al. 2017. Holocene ENSO-related cyclic storms recorded by magnetic minerals in speleothems of central China. Proceedings of the National Academy of Sciences of the United States of America, 114(5): 852–857, doi: 10.1073/PNAS.1610930114

Zong Yongqiang. 2004. Mid-Holocene sea-level highstand along the Southeast coast of China. Quaternary International, 117(1): 55–67, doi: 10.1016/S1040-6182(03)00116-2